Performance evaluation and durability assessment of hybrid alkaline/membrane electrolysis cell designs

Journal of Power Sources 658 (2025) 238239

Contents lists available at ScienceDirect

Journal of Power Sources

journal homepage: www.elsevier.com/locate/jpowsour

Performance evaluation and durability assessment of hybrid alkaline/membrane electrolysis cell designs

Domenico Ferrero [a], Mohsen Mansourkiaei [a], Davide Trapani [a,*], Daniele Consoli [d], Paolo Prevedello [d], Ignazio Assenza [d], Paul Matter [c], Travis Hery [c], Mahtab Fox [c], Alessandro Monteverde [b], Massimo Santarelli [a]

[a] Department of Energy, Politecnico di Torino, Corso Duca degli Abruzzi 24, 10129, Torino, Italy
[b] Department of Applied Science and Technology, Politecnico di Torino, Corso Duca degli Abruzzi 24, 10129, Torino, Italy
[c] Power to Hydrogen Inc., 965 Kingsmill Parkway, Columbus, OH, 43229, USA
[d] Enel Green Power S.p.A, Viale Regina Margherita, 137, 00198, Rome, Italy

HIGHLIGHTS

- Hybrid AEM stack design combining AEMWE with liquid alkaline separator.
- Hybrid design avoids anode exposure to high voltage maintaining membrane hydration.
- Achieved up to 81 % efficiency and 41–46 kWh/kg energy consumption at 1 bar.
- Mechanically supported membranes allow high-pressure operation with low crossover.
- Hundreds of hours of stack tests exhibiting reversible and irreversible degradation.

GRAPHICAL ABSTRACT

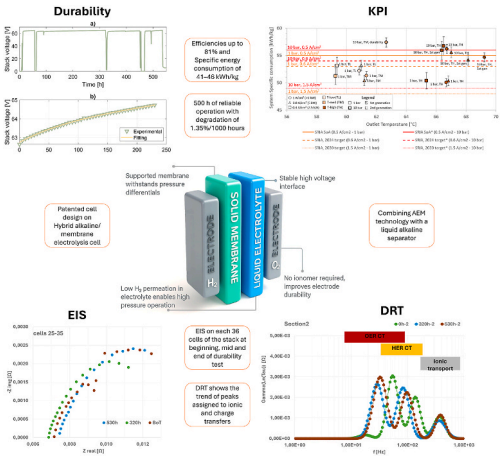

ARTICLE INFO

Keywords:
Anion exchange membrane
Water electrolysis
Hybrid configuration
Durability
oxygen evolution reaction

ABSTRACT

This study explores the performance and durability of a hybrid alkaline/membrane electrolysis cell combining Anion Exchange Membrane technology with a liquid alkaline separator. By leveraging innovative design features, including mechanically supported membranes and hybrid configurations, this approach addresses key challenges in AEMWE systems, such as membrane degradation and limited durability. The hybrid configuration ensures enhanced hydration, minimizes hydrogen crossover, and enables operation under high-pressure conditions, while maintaining high efficiency and low specific energy consumption. Experimental tests were conducted on single cells and stack configurations to evaluate key performance indicators (KPIs), including stack efficiency, specific energy consumption, and hydrogen purity, under varying operational conditions. Results

* Corresponding author.
E-mail address: davide.trapani@polito.it (D. Trapani).

https://doi.org/10.1016/j.jpowsour.2025.238239
Received 2 June 2025; Received in revised form 9 August 2025; Accepted 25 August 2025
Available online 8 September 2025

demonstrated efficiencies up to 81 % at 1 bar and specific energy consumption of 41–46 kWh/kg, nearing 2050 targets for green hydrogen production. In particular, durability assessments revealed both reversible and irreversible degradation processes, and electrochemical impedance spectroscopy (EIS) and distribution of relaxation times (DRT) pinpointed critical performance trends. These findings underline the potential of hybrid AEMWE systems for scalable, cost-effective, and efficient hydrogen production, providing insights into optimization strategies for long-term industrial applications.

1. Introduction

Among electrolysis technologies, Anion Exchange Membrane electrolysis (AEMWE) presents an exciting opportunity, as it combines key advantages from both Proton Exchange Membrane (PEMWE) and alkaline electrolysis (AWE), offering a cost-effective and scalable solution for green hydrogen production [1].

AEMWE leverages a solid polymer membrane similar to that used in PEMWE systems but operates in an alkaline environment. This design allows for the use of less expensive, non-precious metal catalysts and materials, making it a promising alternative to traditional electrolysis methods. AEMWE cells can also be tolerant to water contaminants, avoiding a significant failure mechanism in PEMWE stacks. The alkaline environment also enhances the oxygen evolution reaction (OER) on the anode, enabling more efficient operation. However, traditional AEMWE systems have encountered challenges, especially with durability. The catalyst and ionomers at the membrane-electrode interface tend to degrade over a short period of time [2]. In contrast, membrane degradation typically occurs after several hours of operation [3–5]. Addressing these challenges is essential to scaling up hydrogen production. Various AEMWE configurations have been explored, each with unique advantages and challenges related to water management, system complexity, and performance. Below is a summary of key configurations used in AEMWE electrolysis:

Power to Hydrogen Inc. (P2H2) is an advanced electrolysis company founded in 2019 based in Columbus, Ohio, USA and with offices in Antwerp, Belgium. A hybrid configuration, developed by P2H2, combining various features reported in Table 1, is explored in this work. P2H2 has successfully tackled many of the key challenges in traditional Anion Exchange Membrane (AEMWE) electrolysis by developing a series of innovative solutions, which have significantly enhanced the technology's durability, efficiency, and cost-effectiveness. Their hybrid cell, protected by multiple patents, integrates the advantages of AEMWE technology with a liquid alkaline cell stack, addressing common barriers such as membrane degradation and high operational costs. One of the central breakthroughs comes from P2H2's patented cell design. US Patent 10,844,497 [10] covers a system that integrates an AEMWE with a liquid electrolyte stack, effectively removing the AEMWE from direct contact with the high-voltage interface at the oxygen electrode. This approach mitigates the common degradation problems that have historically limited the lifespan of AEMWE systems. Another key patent, US Patent 11,228,051 [11], involves the use of mechanically supported membranes. These membranes allow for stable operation at high pressures, reducing hydrogen crossover, which is crucial for enhancing both performance and safety during large-scale hydrogen production.

Table 1
AEMWE electrolysis configurations.

Configuration	Description	Advantages	Challenges
Wet Electrodes (Both Cathode and Anode) [4,6]	Continuous liquid electrolyte supply to both electrodes, ensuring full hydration during operation.	Better hydration control, improved reaction kinetics, particularly for the oxygen evolution reaction.	Complex water management and potential risk of electrode flooding if not properly controlled.
Dry Cathode with Liquid-Fed Anode [4,7,8]	Water is supplied to the anode side only, while the cathode relies on water diffusion through the membrane.	Simpler design with easier water management at the cathode.	Difficulty in water transport at high current densities, leading to risk of cathode dry-out.
Pressurized AEM Electrolysis [9]	The cell operates at elevated pressure, enhancing reaction rates and gas purity.	Higher gas purity and faster reaction rates; reduces overall system size.	Requires more durable materials and adds complexity in managing pressure differentials.
Power to Hydrogen hybrid configuration	Hybrid liquid alkaline/AEM cell	Simple system design for pressure balancing, and improved durability versus AEMWE	Non-conventional cell design

P2H2 has also focused on improving the durability of AEMWE systems. Their design uses a liquid electrolyte to maintain constant hydration of the membrane, preventing membrane degradation at high voltages. By strategically isolating the membrane from the harshest operational environments, the system can extend its functional lifespan, making it more reliable and cost-effective for long-term use.

In terms of catalysts, P2H2 has limited use of the costly platinum-group metals (PGMs), typically used in PEM electrolyzers. Instead, they've developed proprietary low-PGM catalysts, optimized for the alkaline environment of AEMWE electrolysis. These catalysts not only reduce costs but also enhance reaction efficiency, making the system both economically viable and highly efficient. Catalysts are deposited on gas diffusion electrodes (GDEs). Carbon paper is used as a support for the cathode catalyst and metal felt is used as a backing layer for the anode. GDEs can be advantageous for AEMWE because it allows electrodes to be reused after a membrane failure. A crucial feature of P2H2's technology is the mechanical support for membranes, which enables high-pressure operation with minimal hydrogen crossover and resistance to pressure differentials. This design not only increases efficiency but also significantly improves durability, allowing the system to handle the demands of industrial-scale hydrogen production.

The review of existing literature shows that most research on AEMWE focuses on the performance of single cells rather than on short-stacks or full system designs. Moreover, these studies often assess durability over relatively short durations, typically around 100 h. For instance, Park Y. et al. [3] conducted a durability test on a 5-cell AEM stack over 150 h at a current density of 0.44 A/cm^2 using 1 M KOH at 50 °C. In these conditions, the stack demonstrated a degradation rate of 2 mV/h, indicating stable, albeit limited, performance. Further, Park S. et al. [12] explored the performance of a 5-cell AEM stack with two different configurations: non-noble metal-based cells except for a Pt cathode (NNM-Pt) and a fully noble-metal-free configuration (NNM). Durability tests conducted for 10 h showed current densities of 1.0 A/cm^2 for NNM-Pt and 0.5 A/cm^2 for the NNM configuration, providing insights into the feasibility of non-noble metal catalysts in these systems. Jang et al. [13]. evaluated the long-term performance of a 3-cell AEM stack, running for 2000 h at 0.5 A/cm^2 with 0.1 M KOH at 45 °C. Over this period, the short-stack voltage increased slightly from 5.04 V to 5.06 V, yielding a degradation rate of 8.5 mV/kh, which translates to a relatively low degradation rate of 0.15 % per 1000 h, indicating promising long-term durability. These studies underscore the importance of extending research to larger stack configurations and longer-term tests to validate the scalability and industrial viability of AEMWE electrolysis.

Recently, Marta Moreno-Gonzalez et al. [14], Chuan Hu et al. [15], and Jun Wang et al. [16] have demonstrated the impressive stability of various AEM membranes, although these studies were performed in a single-cell configuration. However, this configuration may underestimate the impact of mechanical compression, swelling, and current distribution.

The objective of this work is to evaluate key performance indicators (KPIs) and durability at the stack level in a hybrid AEMWE configuration, utilizing a robust design of experiments approach. The ultimate goal is to evaluate reversible and irreversible degradation phenomena, providing insights to guide future operational modes strategies for AEMWE applications.

The work has been carried out in the framework of a collaboration program between industry and research, supported by Enel Green Power S.p.A., involving Politecnico di Torino as technological research organization, and aimed at facilitating the scale-up of promising technologies (Power to Hydrogen Inc. in the present case).

2. Material and methods

Section 2 describes the main characteristics of the cells and stacks developed by P2H2. Moreover, the test protocols adopted to assess the performance, and the durability of the stack are reported. Finally, the test procedure followed for EIS analysis is presented.

2.1. Materials

Active cell components had a circular 100-cm^2 design. The components were manufactured by proprietary methods at Power to Hydrogen Inc, but briefly, the anode was prepared using commercial nickel felt with an ionomer-free nickel oxyhydroxide (NiOOH) layer deposited on the surface. For the cathode, an ink consisting of a low-PGM/carbon catalyst dispersed in water, alcohol, and an ionomer was applied onto a commercial gas diffusion layer (GDL) using an automated spray deposition system. The anode and cathode were then positioned on opposite sides of a commercial anion exchange membrane (AEM), with an additional polymer-based separator layer located on the anode side of the AEM for added mechanical support and separation between the AEM and anode.

2.2. Single cell setup

The cell components were assembled within plastic frames, and compressed using gaskets and bolted endplates, achieving a compression of 30 bar on the cell layers. The endplates included compression gas fittings to feed nitrogen and/or electrolyte to the cells via internal manifolds in the frames, and remove the hydrogen and oxygen product from the cell. Nickel current collectors were used on each end of the cells to apply current, with voltage sensors connected to the current collectors. An electrolyte pump fed electrolyte to the cell. Within this study, two generations of cell designs were evaluated. The only differences between generations were suppliers for the AEM and separator layers, and improvements in electrode quality control.

2.3. Stack setup and test bench facilities

Multiple repeat units of the single cell components were assembled into a hybrid AEMWE stack with an active area of 100 cm^2 for each cell. The stack was constructed using single-serpentine bipolar plates made of stainless steel used on both electrode sides. The complete stack here analyzed consisted of 36 cells connected in series. After assembly the stack, the membrane was activated by circulating KOH, following chloride ion (Cl^-) exchange.

The AEMWE electrolysis test bench was designed for in-depth evaluation of stack and system performance, featuring essential control and monitoring systems. Key components include a heated electrolyte vessel, pressure and temperature controls, a load box, voltage monitoring, mass flow controllers, and separate H_2 and O_2 vents. Key subsystems are:

- **Measurement and Control**: Centralized by a C-Rio (National Instruments, USA) controller, this subsystem acquires and manages data, displayed through an HMI.
- **Gas Management**: Balances pressure between gases and dries the hydrogen
- **Thermal and Water/Electrolyte Management**: Regulates system temperatures and electrolyte supply.

Instruments include a DC power supply, dew point sensor, flow meter, and oxygen transmitter. The system gathers 48 time-stamped signals, covering thermal, power, electrolyte, gas, and actuator parameters for detailed analysis.

2.4. Stack performance assessment

Performance tests on the stacks have been performed to evaluate a set of Key Performance Indicators (defined by Politecnico di Torino and Enel Green Power S.p.A. for the assessment), as listed in Table 2. The test protocol applied to measure the KPIs is described in the Appendix.

The KPI #5 – stack efficiency – has been calculated as:

$$\eta_{stack}^{LHV} = \frac{LHV}{VI} \cdot \dot{n}_{H_2} \quad (1)$$

where LHV is the lower heating value of hydrogen, VI is the stack power measured at the DC power supply, and n_{H2} is the hydrogen flow rate

Table 2
Key performance indicators.

KPI#	Parameter	Unit	Type	Note
1	Current	A	Measured	Measured at power supply
2	Voltage	V	Measured	Measured at power supply
3	Power	W	Measured	Measured at power supply
4	Hydrogen production rate	kg/h or SLPM[a]	Measured	Measured by hydrogen flow meter at dry H_2 outlet
5	Stack Efficiency (DC)	%	Calculated	Calculated (Equation (1)) Measured: hydrogen flow rate and stack power (DC)
6	Stack Specific Energy Consumption (DC)	kWh/kg	Calculated	Calculated (Equation (2)) Measured: hydrogen flow rate and stack power (DC)
7	System Efficiency	%	Calculated	Calculated (Equation (3)) Measured: hydrogen flow rate and stack power (DC)
8	System Specific Energy consumption	kWh/kg	Calculated	Calculated (Equation (4)) Measured: hydrogen flow rate and stack power (DC)
9	H_2 purity (O_2 concentration in the H_2 stream)	ppm	Measured	Measured by oxygen sensor
10	H_2 purity (H_2O concentration in the H_2 stream)	ppm	Measured	Dew point measurement
11	O_2 purity (H_2 in the O_2 stream)	ppm	Measured	Measured by hydrogen catalytic recombiner

[a] SLPM (Standard Conditions: 0 °C and 1 atm).

measured by a hydrogen flow meter.

The KPI #6 – stack Specific Energy Consumption – has been evaluated from hydrogen production rate and cell/stack efficiency as:

$$\epsilon_{stack}^{LHV} = \frac{VI}{(LHV)\cdot\dot{n}_{H_2}} \quad (2)$$

The KPI#7 – system efficiency – and KPI#8 – System Specific Energy consumption – have been calculated as:

$$\eta_{system}^{LHV} = \frac{LHV}{VI + AUX}\cdot\dot{n}_{H_2} \quad (3)$$

$$\epsilon_{system}^{LHV} = \frac{VI + AUX}{(LHV)\cdot\dot{n}_{H_2}} \quad (4)$$

where AUX is the total power consumption of the auxiliary systems of Balance of Plant (BoP) of the stack test bench, calculated as the sum of a fixed contribution (312 W) and a variable contribution (92 % of stack DC power).

It is important to note that the BoP power consumption has not been measured, but it has been calculated using nameplate values of the auxiliary components and assuming the operation profile of each component. Hence, the AUX is representative of a test bench, but does not reflect an optimized system. Consequently, the stack efficiency results are more relevant and comparable to technological targets. Details on the auxiliary components of the test bench and on the assumptions adopted for AUX calculation are provided in the Supplementary Materials.

To design the experiments is necessary to identify the process factors (i.e., stressors) that have a relevant impact on the studied response – the KPIs in the case under investigation. By a preliminary analysis of the technology under investigation and knowing the characteristics of the experimental setup available, two stressors were identified: the stack temperature and the pressure. The preliminary analysis allowed to identify the range of values for the stressors that can be imposed: from room temperature to 80 °C, and from 1 to 30 bar. The higher limits represent the maximum level of the stressor that can be imposed without damaging the stack and compatibly with the testing equipment limits. The primary objective of the experimental campaign was to demonstrate the performance and durability of the stack. To achieve this, performance measurements were conducted prior to the durability testing. To prevent potential damage to the stack before starting the durability assessment, the range of applied stressors was deliberately narrowed. It is important to note that the tests were carried out using a non-commercial prototype test bench. Consequently, to minimize the risk of control-related issues that could compromise the stack, the stressor range was confined to a region of operation that could be reliably managed. In agreement with the stack manufacturer, this precautionary approach was adopted, limiting the stressor values to the following set:

- Stack temperature: 57 °C–62 °C - 67 °C
- Stack pressure (cathodic): 1–10 bar

In the case of the temperature, the values indicated above are the set points, while the real temperature achieved has been measured at the stack outlet as time average during the experiments. The temperature was controlled and monitored at both the inlet and outlet of the anode side the stack. The temperature control system used feedback control to regulate the heating/cooling of the inlet fluid to reach the setpoint temperature, and the system was designed to maintain a $\Delta T < 5$ °C across the stack, minimizing thermal gradients and hot spots. The measured values at the anodic stack outlet – reported in the results – were used for the analysis of the stack performance. In some cases, slight discrepancies between temperature setpoint and time-averaged measured stack outlet temperature occurred, as commented in the results.

Concerning the pressure, the above reported value is the cathodic pressure. The stack operates with a pressure difference of 1 bar between cathode and anode. This $\Delta P = 1$ bar configuration ensures cathode overpressure to suppress oxygen crossover, without inducing excessive stress on the membrane. The higher pressure value selected of 10 bar cathode (i.e. 9 bar anode) was based on safety and performance trade-offs. Pressure values were monitored with calibrated transducers and remained within ±0.1 bar of setpoints. Similar pressurization strategies have been reported in pressurized AEMWE studies [17].

The experiments have been designed following a Design of Experiment (DoE) approach applying a response surface design (Box–Behnken type design), that allows to identify the relation between experimental response (directly measured or calculated from experimental results) and input parameters of the test. The DoE approach selected is a Central Composite Design of the Central Composite Inscribed design (CCI) type. However, not all the planned points were tested due to time restrictions. The plan of the stack tests for the evaluation of the KPIs is summarized in Table 3, in which $P_{low} = 1$ bar and $P_{high} = 10$ bar is the stack pressure (cathode pressure). The temperatures indicated in the table are setpoint temperatures imposed to the stack. Each test included 3 repetitions measurements at 0.4 A/cm^2 (2.5 kW), 0.8 A/cm^2 (5 kW) and 1 A/cm^2 (~6.5 kW). The tests were performed both on the stack assembled with the first generation of cells and on the one employing the second generation.

Statistical methods have been applied to the analysis of the experimental results obtained. In general, the relation between each KPI (i.e., the studied response of the experiment) and the two stressors can be determined with the adoption of a second-degree model to take into account non-linear and cross-variables effects. The model is of the type:

$$Y = a_0 + \sum a_i X_i + \sum a_{ij} X_i X_j + \sum a_{ijk} X_i X_j X_k + \sum a_{ij} X_i^2 \quad (5)$$

where Y is the studied response that is the sum of the contribution of the constant effect, the linear effect, the second order interactions effect, the order k interactions effect and the possible quadratic effect. Due to the limited range of the stressors in the performed experiments, a multilinear regression has been selected after the correlation between the parameters has been verified and the multicollinearity excluded (see section 3.1.3). The regression model for the stack and system specific consumption is reported in the results.

2.5. Durability protocol

The durability test aimed at assessing the performance degradation over 1000 h of continuous operation in the following conditions:

- Current density: 1 A/cm^2
- Operating temperature: 62 °C
- Operating pressure: $pH_2 = 10$ bar and $\Delta p = 1$ bar (i.e., $pO_2 = 9$ bar)

We have operated the durability for approximately 500 h, and then we have developed an extrapolation to 1000 h to be consistent with the indications of the test protocol proposed by the Joint Research Center (JRC) [18].

The operating current, the stack power and the stack temperature were continuously monitored during the long-term operation. The

Table 3
Plan of stack tests.

Stack	Temperature [°C]	Current Density [A/cm^2]	Pressure [bar]
First Generation	67	0.4-0.8-1	10
Second Generation	57-62-67	0.4-0.8-1	1
	62[a]	1[a]	10[a]
	67	0.4-0.8-1	10

[a] Point measured at the beginning of durability test at 1 A/cm^2, no repetitions.

experimental data were recorded with a time resolution of 5 s and the hourly average values were then calculated.

The experimental data were fitted and extrapolated to estimate the increase in the stack voltage after running the system for 1000 h, which represents the reference number of hours recommended for long-term testing by well-established and harmonized test protocols [18,19].

In the existing literature, different fitting curves are adopted to investigate the long-term operation of electrochemical devices (i.e., fuel cells and electrolyzer) and the consequent degradation phenomena. Specifically, Xing et al. in Ref. [20] proposed a linear fitting approach to investigate the long-term durability of membrane electrode assemblies for AEM electrolyzer. In this case, the voltage evolution over time is expressed as in Equation (6):

$$V(t) = a \cdot t + b \tag{6}$$

Conversely, Gazdzick et al. in Ref. [21] presented a linear-exponential function with the aim of considering both reversible and irreversible degradations. The reversible degradation is described by the linear term, while the irreversible degradation is expressed by the exponential part. The fitting function was initially formulated for PEM fuel cells, but in the present study it was properly adapted to the electrolyzer operating mode while preserving the same rationale. The voltage increase over time is thus expressed as in Equation (7):

$$V(t) = a \cdot t + b + c \cdot (1 - \exp(-t / d)) \tag{7}$$

The fitting analysis was performed by using the Curve Fitter app, which is included in the Curve Fitting Toolbox 3.8 in MATLAB 2022b. The fitter tool adopts the method of the least square minimization and provides as output the values of the fitting coefficients and R^2, which indicates the goodness of the fit.

The extrapolation procedure consisted in estimating the stack voltage ($V_{1000,fit}$) that would be reached after 1000 h of continuous operation. Based on the outcome of these procedures, the percentage increase in the stack voltage after 1000 h of operation was calculated as:

$$\Delta V_{1000} = \frac{V_{1000,fit} - V_{BoI,real}}{V_{BoI,real}} \cdot 100 \tag{8}$$

In which $V_{1000,fit}$ represents the extrapolated voltage value after 1000 h of operation and $V_{BoI,real}$ corresponds to the voltage value measured at the beginning of the test/test interval.

2.6. EIS

Electrochemical impedance spectroscopy has been done during the durability test in order to evaluate the stack at specific points of operation. Tests have been performed using Gamry instrument's Interface 1010 E (Gamry Instruments, USA) which has the following key characteristics:

- Max Applied Current ±1 A
- Maximum Applied Potential ±12 V
- EIS 10 μHz - 2 MHz

Fluke 2638A hydra instrument (Fluke, USA) is used on each of the 33 cells of the stack separately through tabs connected to the monopolar or bipolar plates at the following time steps: beginning of tests (BoT), after 320 h of durability test, after 530 h.

A specific testing protocol was followed for all the tests. The protocol was partially adopted from ANIONE EU project [19]. For each of the mentioned four stages of the experiment, every one of the 36 cells of the stack has been tested for galvanostatic impedance spectroscopy using the potentiostat instrument. During EIS, the cells were kept in nominal point of operation at atmospheric pressure and the electrolyte flow was kept constant in the nominal range while the temperature was kept in the range of 55–60 °C. The experiments were done with an initial frequency of 10^4 Hz and final frequency of 1 Hz keeping 7 points per decade and with a 1.5V DC potential.

3. Results and discussion

3.1. KPIs

3.1.1. Stack tests

The KPIs evaluated from the stack tests performed on the first-generation stack are reported in Table B1 (see Appendix B). Each one of the KPIs reported in the Table is the average data of 3 repetitions, excluding the values of the column P1, which are the average data of 2 repetitions. The results refer to a stack performance at 10 bar and a temperature close to 70 °C. The stack temperature - measured at the anodic outlet of the stack - shows values increasing with the stack current, as expected from the increase of stack losses at higher current. The stack efficiency ranges from 72.8 % (P1) to 69.5 % (P3), with a stack electricity consumption increasing almost linearly with the stack outlet temperature in the range 45–48 kWh/kg.

At system level, the efficiency ranges between 59.5 % and 61.4 %, while the system electricity consumption is in the range 54–56 kWh/kg. As previously commented, the system efficiency is representative of a non-optimized system, and it is affected by the assumptions adopted for the estimation of the BoP power consumption. In particular, the BoP consumption is more affecting the system consumption when the stack is at low power, due to the higher weight of the fixed contribution, and for this reason the system specific consumption exhibits a different trend compared to the stack consumption.

The KPIs evaluated from the stack tests performed on the second-generation stack are reported in Table B.2 and Table B.3. Each of the KPIs reported in the previous tables is the average of 3 repetitions, excluding the values reported for the 10 bar test @62 °C, which are the average data of the first 20 min of the durability test, and the P2 and P3 values of the 1 bar test @67 °C (see table notes). The stack tests have been equally distributed on the 3 levels of current (excluding the beginning of durability point that is available only at 1 A/cm^2) and were performed at 2 levels of pressure and at measured outlet stack temperatures that are distributed between 59 °C and 67 °C.

The results of stack tests are summarized in Fig. 1 (upper panel) in terms of stack specific energy consumption vs. temperature measured at the outlet of the stack. In the figure, the values of stack specific consumption calculated at 0.4, 0.8 and 1 A/cm^2 – excluding the point from durability test, for which only the 1 A/cm^2 point is available – are reported. The three tests at 1 bar reported in the figure have been performed with different stack temperature setpoints (T_{low}, T_{mid} and T_{high}, see Table 3). It is worth noting that the tests at 1 bar with T_{low} and T_{mid} (orange and grey points on the figure) setpoints achieved very similar measured stack outlet temperatures, highlighting some limitations of the testing setup of controlling the stack temperature in a narrow range of temperature setpoints.

In the figure, it is clearly visible the dependency of the stack efficiency on the pressure, with the tests at 10 bar (symbols outlined with a thicker black edge) having a lower efficiency. Energy consumption increases with operating pressure for all the three levels of current density. In particular, tests at 1 bar show a stack efficiency in the range 72 %–81 %, and a specific consumption in the range 41.2–46.1 kWh/kg, while the 10 bar tests are in the ranges 66 %–72 % and 46.4–50.3 kWh/kg.

It is also evident from tests conducted with a power of 2.5 kW (square points on the Fig. 1 – upper panel) that the electrolyzer has low electrical consumption compared to the operating points at higher power of the same tests, that is typical of electrochemical systems operating at a non-nominal point, thus warranting consideration of an oversizing factor. In particular, tests at 2.5 kW and 1 bar have an average stack specific consumption of 42.2 kWh/kg compared to 44.4 kWh/kg and 44.9 kWh/kg for the 5 kW and >6 kW test, respectively. It is important to emphasize that international electricity consumption targets for

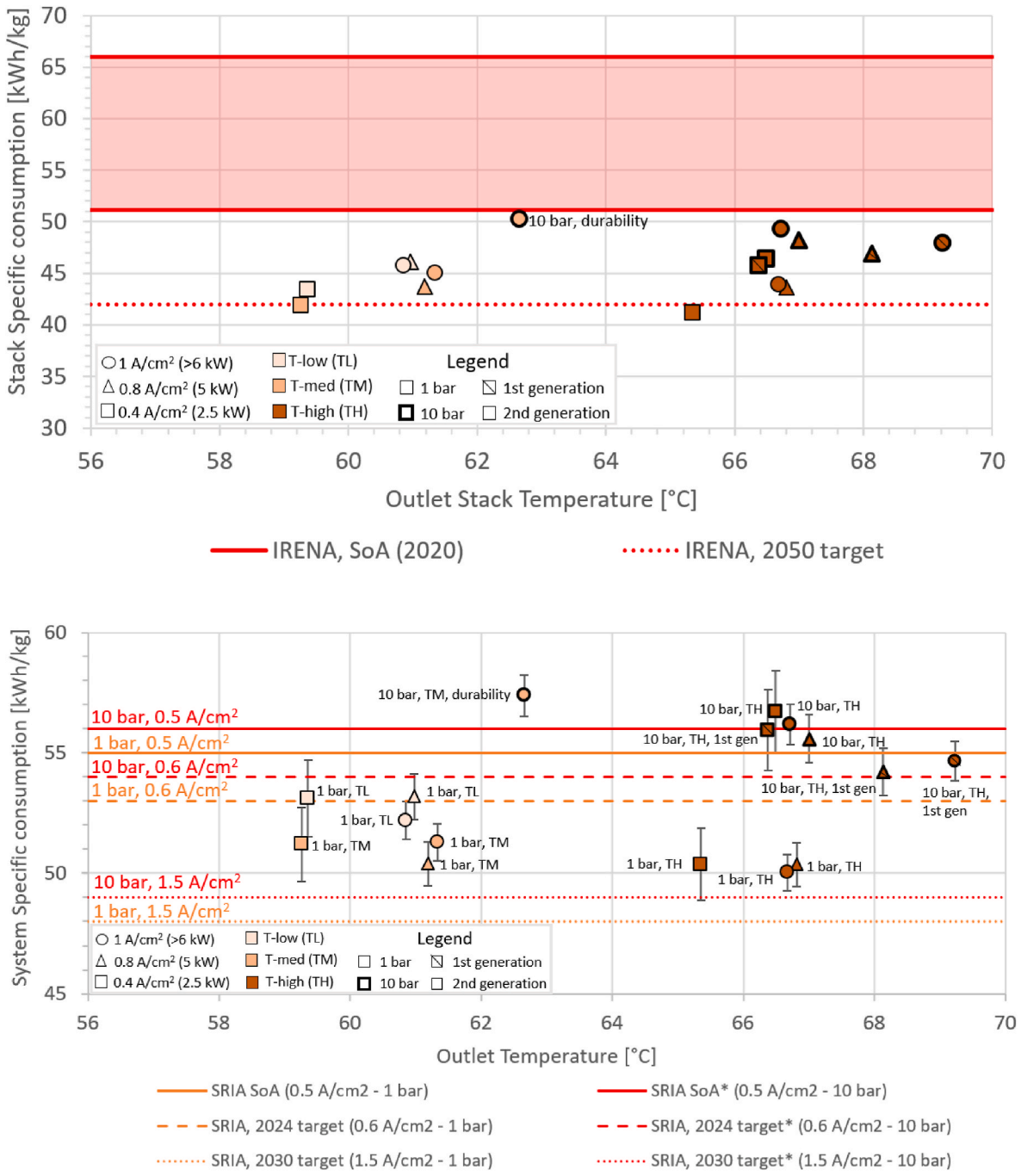

Fig. 1. Upper panel: stack specific consumption of 1st and 2nd generation compared with SoA and 2050 target (IRENA 2020); lower panel: system specific consumption of 1st and 2nd generation stack tested on test bench (BoP not optimized) compared with SRIA system targets and adjusted at 10 bar (labelled with *) SRIA system targets.

electrolysis usually refer to specific consumption under nominal conditions; therefore, data at a partial load of 2.5 kW are of little relevance for comparison.

The stack efficiency shows a limited relation with the temperature. It is worth highlighting that the stack outlet temperature shown in the graph is not only affected by stack losses, but also by the inlet stack temperature, which was varied during the tests to maintain a stack setpoint temperature. Moreover, the points analyzed are in a narrow range of temperatures. When considering the tests performed at 1 bar, the data have comparable trends with the temperature. Observing the graph, for each group of tests at 1 bar at a certain fixed setpoint temperature, the point at 2.5 kW shows lower outlet stack temperature and efficiency compared to the 5 kW and >6 kW points, which show similar efficiencies at temperatures around 2 °C higher in all the cases analyzed. When comparing all the different tests, in general a slight decrease of the stack consumption with the temperature can be found comparing all the points at 1 A/cm^2 (also for the 10 bar tests). The observed trends are suggesting a rising thermal profile indicative of efficiency decrease with the increase of the current density and, conversely, an increase in kinetic activity due to temperature rise (Arrhenius trend). When considering the tests at 10 bar, the energy consumption trend is less consistent with the observed variability in temperature.

The results of system tests are summarized in Fig. 1 (lower panel) in terms of system specific energy consumption vs stack outlet

temperature. All the tests summarized in Table 3 are reported in the figure. The system consumption is due to BoP auxiliaries and it is assumed as composed by a fixed contribution and a variable part that is proportional to the stack power (see Section 2.4). For this reason, the BoP consumption is more affecting the system consumption when the stack is at low power, due to the higher weight of the fixed contribution. In particular, 1 bar tests show a system efficiency in the range 63 %–66 % (50.3–53.2 kWh/kg) for both 2.5 kW and 5 kW test and 64 %–67 % (50.0–52.2 kWh/kg) for the >6 kW. As expected, the nominal operating points at 1 A/cm^2 have on average a better system performance, even if the one point (1 bar test at 62 °C setpoint temperature) shows a higher efficiency at 5 kW, but this is due to the better stack performance, as shown by stack results.

It is worth highlighting that the 10 bar durability point shows a higher energy consumption (and a lower efficiency) that the other points both at stack and – consequently – at system level.

Concerning other measured system parameters, the hydrogen purity at the outlet in terms of oxygen concentration is in the range of 30–170 ppm for the 1 bar tests and in the range of 8–45 ppm for the 10 bar tests. In the case of 1 bar tests, the oxygen concentration shows a decreasing trend with the increasing stack current. In particular, at 2.5 kW the O_2 concentration is in the range 113–168 ppm, at 5 kW is in the range 66–100 ppm and at >6 kW is in the range 38–96 ppm. At 10 bar the trend is comparable for the 3 tests performed at 67 °C of nominal temperature, with the oxygen concentration decreasing from 27.9 ppm to 8.7 and 8.2 ppm with the increasing current. The 10 bar durability test shows an higher concentration (44 ppm), which is closer to the one of the first-generation stack tests (10 bar and 70 °C) that is around 32 ppm and it is not affected by the stack power.

Concerning the humidity content of the hydrogen, it is in the order of 10^4 ppm and its value is not clearly related to stack temperature, pressure and current.

3.1.2. Regression model

A regression model for the second-generation stack performance has been derived, using the DoE approach, from the measured data. The second-generation stack has been selected for the development of a regression model due to the larger number of available measured points.

The regression analysis has been focused on the stack performance because it is directly affected by the pressure, temperature and power (or current) parameters, while the system performance is also affected by BoP auxiliaries consumption that cannot be clearly put in relation with the abovementioned parameters. In addition to this, the BoP of the P2H2 system is not optimized, but it is only a system suitable for the stack testing.

Due to the limited range of the parameters, a multilinear regression has been selected.

As a first step, the correlation between the parameters has been verified (details are reported in Supplementary Materials). A relevant correlation between the stack specific consumption, the temperature, the power and the pressure is found. There is also a correlation between the stack temperature and pressure; however, this is not due to the physics of the system, but because the 10 bar tests were performed mostly in the higher temperature range, while the 1 bar tests at all the temperatures. Thus, multicollinearity can be excluded. The multicollinearity analysis between Temperature, Power and Pressure indicates a negligible correlation between the parameters (see details in Supplementary Materials). Thus, Temperature, Power and Pressure can be considered independent parameters for the regression.

The multilinear regression has been performed, identifying the following function to put in relation the stack specific consumption (Y) and the temperature (T), the stack power (P) and the pressure (p):

$$Y = 54.42 - 0.24\,T + 0.00080\,P + 0.57\,p$$

The function has an $R^2 = 0.94$ (close to 1) proving the goodness of the fitting function. The results are shown in Fig. 2.

3.1.3. Analysis of system specific consumption KPIs vs. international targets

The specific consumption of the stacks is reported in Fig. 1 (upper panel) compared with the State-of-the-Art (SoA) range – red area in the figure – and the 2050 target indicated by IRENA for the AEMWE technology [22]. The figure includes all the tests at 1 A/cm^2 summarized in Table 3. The figure shows three points for the 1 bar test on the second-generation stack, each representing a test conducted at different temperature.

The SoA (2020) efficiency of AEMWE stacks estimated in the report of IRENA is the range 51.5–66 kWh/kg and a value < 42 kWh/kg is reported as 2050 target. The SoA range refers to stacks operating in the current density range of 0.2–2 A/cm^2 and at pressure <35 bar, while the 2050 target is for stacks operating at > 2 A/cm^2 and a pressure >70 bar. The measured electrical efficiency of the stacks tested (both 1st and 2nd generation) falls already below range of the SoA values, with the tests at lower pressure and higher temperature showing a better performance. In particular, the stack specific consumption of the test performed at 1 bar

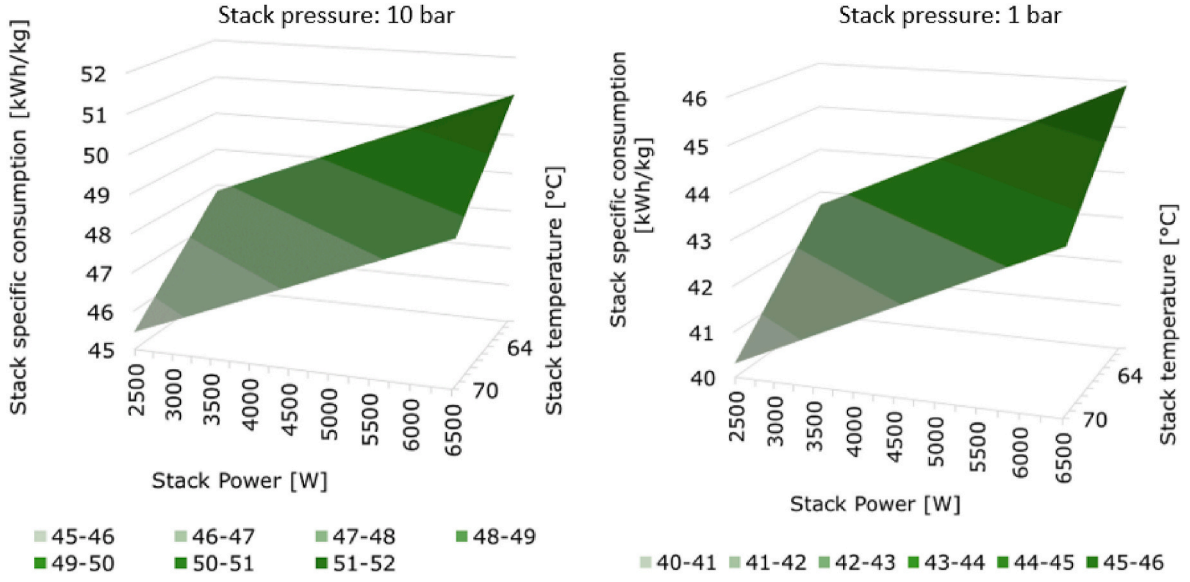

Fig. 2. Regression surface @10 bar (left panel) and @1 bar (right panel).

and around 67 °C is around 44 kWh/kg, already close to the 2050 target, even if this target refers to stacks operating at higher current density and pressure.

The system specific consumption that has been evaluated for the 1st and 2nd generation stacks is reported in Fig. 1 (lower panel) compared with the electricity consumption Key Performance Indicator for AEMWE of the Strategic Research and Innovation Agenda (SRIA) of Clean Hydrogen JU [23]. As in the case of stack specific consumption, the figure shows three points for the 1 bar test, each representing a test conducted at different temperature.

The SRIA values reported for the AEMWE technology are: 55 kWh/kg as SoA (2020), 53 kWh/kg as 2024 target, and 48 kWh/kg as 2030 target. These KPI values are defined for a system that produces hydrogen at atmospheric pressure and are referring to a SoA (2020) current density of 0.5 A/cm^2, and target current densities of 0.6 A/cm^2 and 1.5 A/cm^2 in 2024 and 2030, respectively. In particular, standard boundary conditions of SRIA that apply to all system KPIs assume as input AC power and tap water and the output of hydrogen meeting ISO 14687-2 at atmospheric pressure and hydrogen purity 5 [23]. As the SRIA targets are defined for hydrogen produced at atmospheric pressure, the electricity consumption of a system operating at 10 bar should be compared with adjusted SRIA targets to take-into-account the hydrogen compression from ambient pressure to 10 bar. If we consider an ideal compression of the produced hydrogen flow (isentropic and adiabatic compression at 20 °C from 1 bar to 10 bar), a value of ~1 kWh/kg for the hydrogen compression can be estimated. Thus, the SRIA targets can be adjusted considering 56 kWh/kg as SoA (2020) for the system (i.e., 55 kWh/kg + 1 kWh/kg for the compression) and 54 kWh/kg (i.e., 53 + 1) as 2024 target and 49 kWh/kg (i.e. 48 + 1) as 2030 target. All the SRIA targets and the corresponding adjusted values are reported in Fig. 1 (lower panel) as horizontal lines.

Concerning the 1st generation stack, it has a specific consumption of 54.65 kWh/kg. This is a better performance than the State-of-the-Art (2020) SRIA target for the AEMWE electricity consumption, which is 55 kWh/kg.

It is worth highlighting that the results here measured are better because:

- the SRIA value refers to atmospheric pressure hydrogen, while the stack is producing hydrogen at 10 bar;
- the data of the system here measured are obtained at a current density of 1.0 A/cm^2.

When compared to the adjusted SRIA targets, the system efficiency of the 1st generation stack (54.65 kWh/kg) is also very close to the 2024 target (54 kWh/kg).

It must be outlined again that the system results reported in the figure for both 1st and 2nd generation stacks include experimental data of the stacks and the estimated BoP consumption of the test-bench used to test the stacks (same test-bench for both stacks). The BoP is designed for testing, but not optimized, and the estimation of the BoP components consumption has been made using the nameplate data of the components and a realistic profile of their use (steps with fixed fraction of nominal power and duration) during the stack test (see Supplementary Materials).

Taking-into-account all these considerations, it can be stated that the performance of the first-generation stack is well in line (or even already better) with the 2024 SRIA targets for AEMWE.

When considering the 2nd generation stack, at 10 bar it achieved a specific consumption of 56.2 kWh/kg and 57.4 kWh/kg (beginning of durability test). These values are higher than both the adjusted SRIA SoA (2020) value and the consumption of the 1st generation stack.

Concerning the 2nd generation stack tested at 1 bar, the 3 values reported are already lower than the SRIA target for 2024 (53 kWh/kg), but still far from the 2030 SRIA target of 48 kWh/kg. Among them, test performed at the higher stack temperature has a specific energy consumption very close to 50 kWh/kg.

Also for the 2nd generation stack are valid the same considerations on current density and not optimized BoP done for the 1st generation stack.

3.2. Durability

Fig. 3a depicts the stack voltage evolution during the durability test, which was performed at a constant current density of 1 A/cm^2.

The stack was successfully operated for an accumulated period of 482 h. However, some unplanned test interruptions occurred during the long-term operation, resulting in five distinct test intervals. The duration of each test interval is reported in Table 4.

The durability test thus experienced multiple stops and restarts. However, it is worth noting that these interruptions were not due to stack damage, but they were instead caused by procedural error, power outage and computer failures. Despite these issues, the stack thus proved to be reliable and capable of operating continuously for hundreds of hours, as confirmed by the duration of test interval #3 and #4 (230 and 119 h, respectively). The analysis of the durability data thus focused on test interval #3 as it represents the longest test period without interruptions. The experimental data were fitted and extrapolated according to the methodology described in Section 2.5.

The coefficients of the linear-exponential fitting and the results of fitting and extrapolating procedures are summarized in Table 5.

Fig. 3b shows the fitting of the experimental dataset recorded during the 230 h of operation. The graph highlights that the fitting curve accurately matches with the measurements, as confirmed by the high R^2 value. Fig. 3b illustrates the extrapolated trend of the stack voltage, which reaches 68.09 V after 1000 h of continuous operation. According to this extrapolation trend, the percentage degradation rate would result in 8.7 %/1000 h.

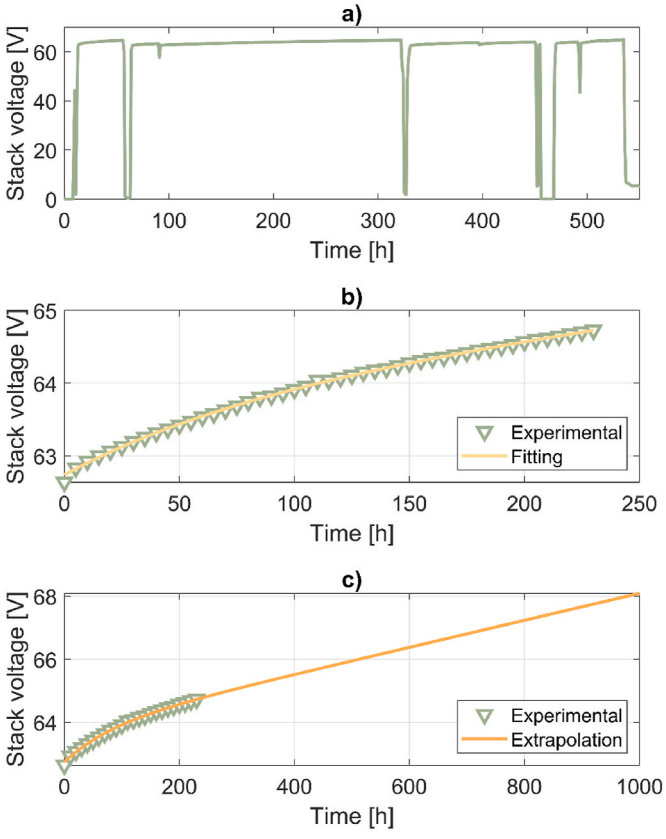

Fig. 3. a) Stack voltage evolution over long-term operation; b) Linear-exponential fitting; c) Linear-exponential extrapolation.

Table 4
Durations of test intervals and interruptions.

Test interval	Duration [h]
1	43
2	25
3	230
4	119
5	65

Table 5
Coefficients for the linear-exponential fitting.

Parameter	Value
a	0.004285
b	62.74
c	1.066
d	82.96
R^2	0.9992
$V_{BoI,real}$	62.64
$V_{BoI,fit}$	62.74
$V_{EoI,real}$	64.73
$V_{EoI,fit}$	64.73
$V_{1000,fit}$	68.09
ΔV_{1000}	8.7 %

The estimated degradation rate is thus compared with the target and the existing literature. The current European target for degradation of SoA AEMWE electrolyzer is >1 % over 1000 h of operation, while the target for 2024 and 2030 is set to be lower or equal to 0.9 and 0.5 % over 1000 h, respectively [24]. The degradation rate estimated based on the 230 operating hours results in line with SoA electrolyzers, but it exceeds the 2024 target. Nevertheless, it is worth highlighting that the test conditions applied in the long-term operation (i.e., 1 A/cm^2, operating pressure of 10 bar, operating temperature of 62 °C) have been very rigorous. In fact, according to Li et al. [25], most of the durability assessments of AEM cells are performed with less severe test conditions (e.g., low current density, low operating temperature and ambient pressure). Furthermore, Titheridge and Marshall in Ref. [26] emphasized that in absence of standardized testing procedures, the results of electrolyzer testing can vary significantly and they cannot be directly compared. In addition, Du et al. in Ref. [4] stated that different cell design (e.g., catalyst type and loading, membrane and electrolyte) and distinct test conditions make the comparison of durability performances not straightforward. Indeed, they listed the relevant durability studies available in literature as of 2022 reporting degradation rate in a wide range of 5–2571 μV/h, which correspond respectively to 0.26 % and 139 % increase over 1000 h.

In Fig. 4a the stack voltage at beginning of interval (BoI) and end of interval (EoI) for the different test intervals are reported. As is evident, a performance degradation occurs while operating the system in long-term mode (in each interval, there is a difference between voltage value at BoI and EoI). According to Du et al. [27], the formation of bubbles may represent one of the main phenomena affecting the stack performance. However, at each system restart (BoI of every single interval) a significant fraction of the overvoltage is recovered (i.e., a sort of reversible overpotential, probably due to the bubbles formed during operation as analyzed by Du) and the performances are restored [27]. The largest overvoltage recovery is recorded after the test interval #3, which has the longest duration (i.e., 230 h). Specifically, at the beginning of the test interval #4, the stack voltage stands at 62.44 V, which is comparable to the voltage values measured at BoI #2 and #3. At the beginning of test interval #5 (i.e., after 349 h of operation in test interval #3 + #4), a permanent degradation (not recovered anymore) can be pinpointed: the stack voltage thus results around 63 V, which results higher compared to the previous BoI values (that are in the range 62.3–62.6 V). When considering the whole test phase, the stack voltage

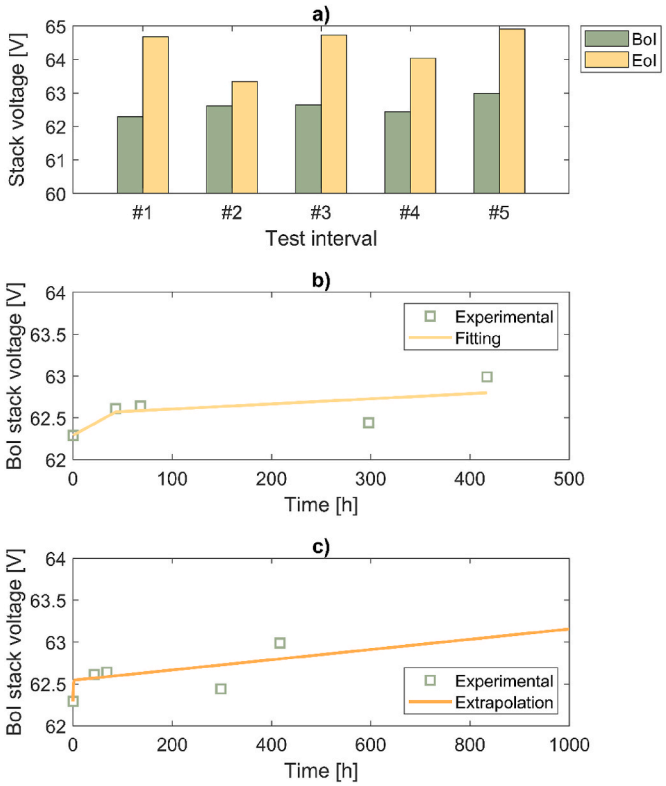

Fig. 4. a) Stack voltage at BoI and EoI for the different test intervals; b) BoI stack voltage fitting; BoI stack voltage extrapolation.

rises from 62.3 V (green value) to 64.9 V (yellow value), but only to 63 V (green value), over 482 h of testing.

With the aim of considering the positive effect of the voltage recovery caused by a system stop and restart and thus assessing only the irreversible degradation, the fitting of the BoI stack voltage values was performed adopting the linear-exponential trend. The results of the fitting procedure are shown in Fig. 4b.

The voltage evolution over time was thus extrapolated and the stack voltage after 1000 h was estimated in 63.13 V, as shown in Fig. 4c. Thus, when considering only the permanent degradation, the percentage increase of the voltage results in 1.35 %. In this case, the degradation rate estimated based on the BoI stack values is close to the 2024 target. It is worth noting that this value is calculated compared to the stack voltage value measured at the beginning of the test interval #1. In addition, it is necessary to emphasize that the interruptions which occurred during the 500 h of operations were neither planned nor periodic. Consequently, this estimated degradation does not refer to a specific operating strategy. Further, in single-cell tests (data not shown) most degradation occurs in the first 500 h of operation (i.e. the break-in period) before stabilizing. Future work is planned to test beyond 500 h.

The analysis of the different test intervals revealed that a notable portion of the degradation was reversed after pausing and restarting the system. However, a direct correlation between pause duration and voltage recovery was not observed, possibly due to other factors (e.g., pump leakage and electrolyte refresh) affecting the performance recovery. Thus, it appears clear that running the electrolyzer at a variable current and with intermittent operation (e.g., when driven by a photovoltaic field with fluctuating current levels during the test) results in a lower degradation rate compared to the operation at a constant and relatively high current (i.e., 1 A/cm^2). Specifically, constant operation leads to a degradation rate 6.44 times larger than intermittent operating mode (i.e., 8.7 % versus 1.35 %).

3.3. EIS test on the stack cells

In order to evaluate the results of EIS four steps have been performed in this section. Firstly, the data quality has been studied. As the second step the data presentation and analysis has been done using the Nyquist plots. Subsequently electrical equivalent circuit was derived for the spectra and finally distribution of relaxation times was analyzed.

3.3.1. Data quality and validation analysis (Kramers-Kronig)

The validity of all analysis using the EIS data relies on the measured spectrum representing a linear, time-invariant and causal system. To assess data validity, Kramers-Kronig (KK) numerical analysis is employed, which consists of a set of transformations that predict one component of impedance from the other over the theoretical frequency range from zero to infinity. To reduce complexity and efficiently verify causality, linearity, and stability, the linear KK method introduced by M. Schönleber et al., based on the work of B. A. Boukamp [28,29], was utilized. The analysis has been performed using linear Kramers-Kronig with a complex fitting. Residuals of fitting the real and imaginary data is brought in Fig. 5a. According to Schönleber et al., a residual within ±0.5 % indicates high-quality data. In this study, approximately 94 % of the measured data exhibited residuals below 0.5 %, while only 0.6 % of the data—equivalent to 2 out of 310 samples—had residuals exceeding 2 %, as detailed in the supplementary materials. The small subset of data with higher noise has been recorded mainly at the start of the durability test -0h-while the rest of the data show very good quality with residuals well below 0.5 %.

3.3.2. Nyquist plot

Considering the three stages of the tests namely, the beginning of test (BoT), 320 h, and 530 h the results of test on each cell within the stack at these time steps can be presented in three separate Nyquist plots. Fig. 5b refers to the Nyquist plot of the EIS results at 320 h of test for cell 1 to 36 excluding the positive portion of the imaginary impedance values which is typically attributed to the inductive behaviour of the cables. As observed in the graph, apart from cells 1 and 36- which utilise thicker plugs for cable connection -the remaining cells exhibit similar curve shapes, indicating the homogeneity of the cells. Given the large number of acquired data points, the stack cells have been grouped into three clusters to facilitate comparison and ensure clearer data presentation. Due to the variations in electrical plug connections for the first and last cells, and in order to maintain consistency within the clusters, cells 1, 2, and 36 have been excluded from the main graphical analysis, resulting in three groups of 11 cells each. However, for completeness and accuracy, the spectra of cells 1, 2, and 36 at 320 h of testing are provided in Fig. 5 as a reference. Thus, the stack is divided into three cluster cells: Cluster 1 including cells 3 to 13, cluster 2 having cells 14 to 24, and cluster 3 containing cells 25 to 35.

For the mentioned clusters, the Nyquist graphs are reported in Fig. 6. As seen in the graphs, there is an overall increasing trend in the real-axis intercept (Z_{Real}) as well as an overall change in the size of the semi-circles in the graphs from the BoT to the end of test (EoT). Based on the physical characteristics of the cells and the experimental results, an equivalent circuit with an inductor, an ohmic resistance and two blocks of constant phase elements (CPE) and resistances – each of two depicting the double layer capacitance and charge transfer resistance of an

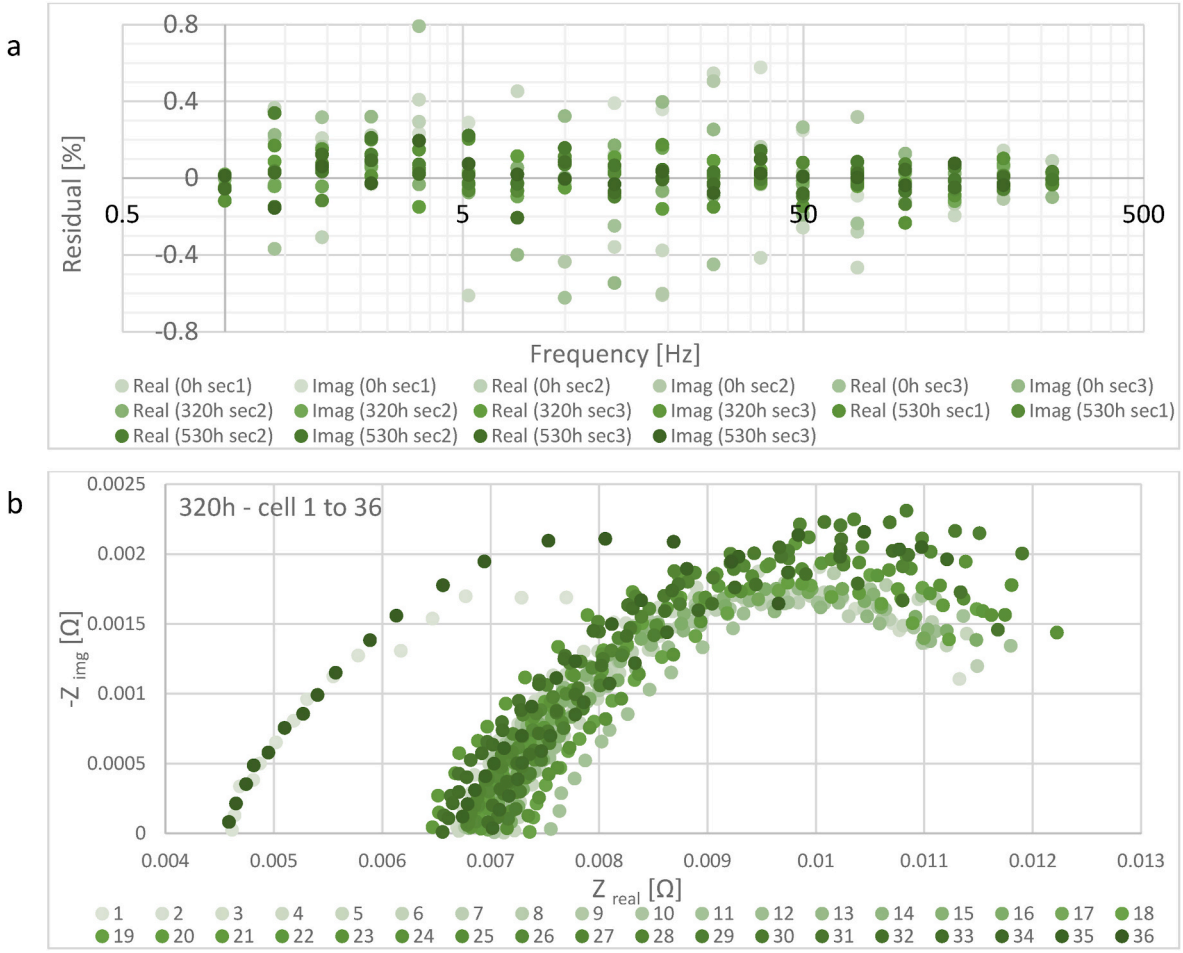

Fig. 5. a)KK residuals of Imaginary and real fittings of EIS spectra (Top); b)Nyquist plot of the EIS at 320h for the stack. Each series refers to the relative cell number of the stack. Each data series refers to the same cell number in the stack (Bottom).

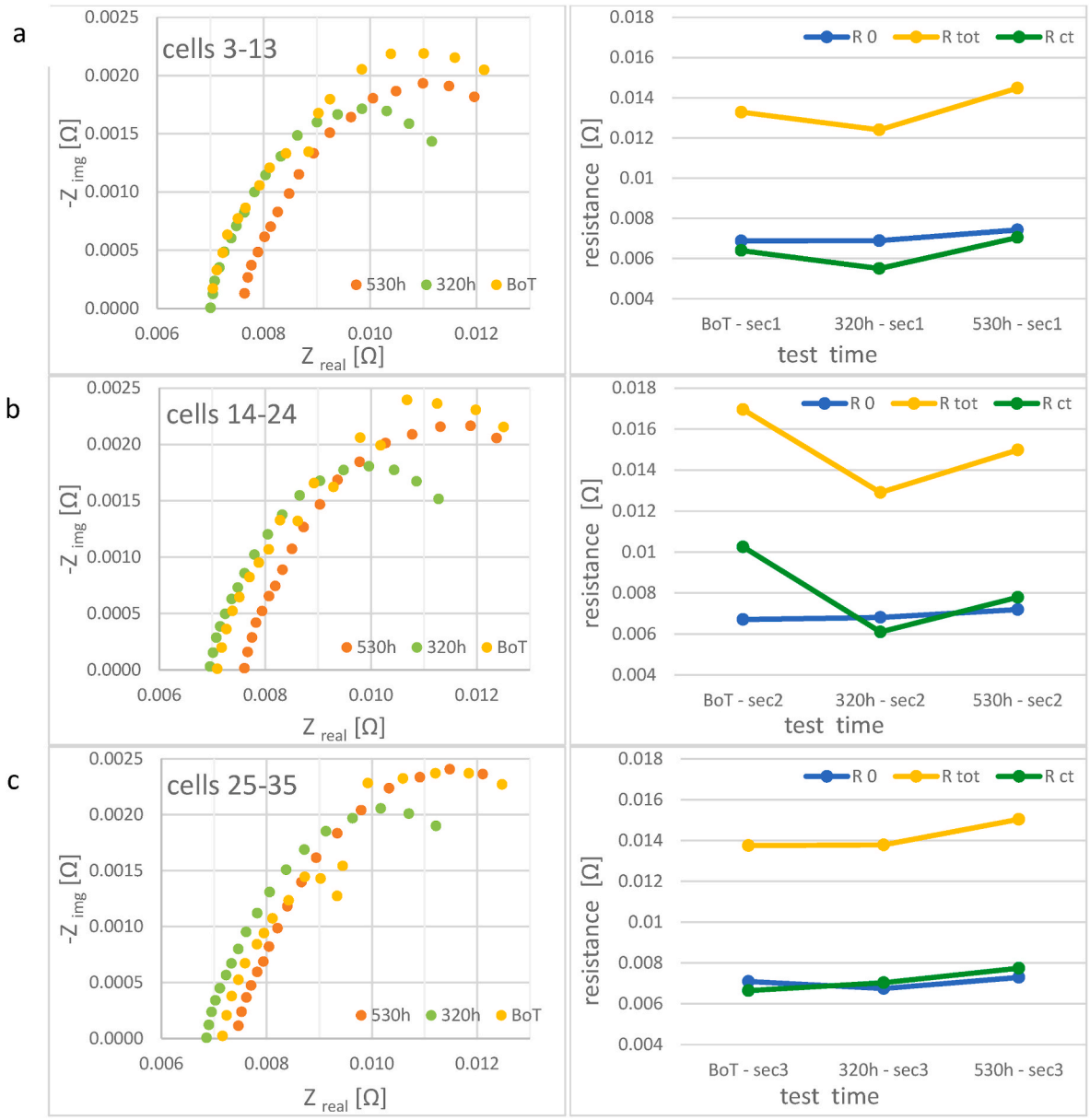

Fig. 6. Nyquist plot of the average results of the three cell sectors and their relative fitted resistances from EEC of the three cell sectors. a) cells 3–13, b) cells 14–24, c) cells 25-35.

electrode-were used to electrically simulate the system's behaviour. This circuit can be seen in Fig. 7a.

3.3.3. *Electrical equivalent circuit (EEC): ohmic resistance (R_0), total resistance (R_{tot}) and charge transfer resistance (R_{ct})*

To improve the data quality, it is possible to exclude the inductive-resistive section of the Nyquist plot when analyzing the spectra in equivalent circuit model. Consequently, the positive imaginary part of the Nyquist graph has not been considered in this analysis. The results of electrical equivalent circuit models are presented in Fig. 6 alongside their corresponding Nyquist graphs. In these graphs the absolute values of resistances are reported. R_{ct} is the sum of R_a and R_c contributions while the total resistance is the sum of ohmic and polarization resistances.

For the ohmic resistance, an overall increase can be observed throughout the tests. In comparison with the results of previous initial single cell tests that have been performed on similar cells of the stack, the ohmic resistance value shows same order of magnitude (mainly in the range of 0.006–0.007 [Ω]) confirming the repeatability and reliability of the test results for the stack cells. In the third stack sector, a slight improvement is observed during the first 320 h of the experiment; however, the overall trend remains degradative. The percentage increase in ohmic resistance is reported in Fig. 7b.

Using the chosen electrical equivalent circuit model, the charge transfer resistance R_{ct}, and total resistance R_{tot} for the three sections of the stack can be determined. These resistances are shown in Fig. 6 and as it can be seen the overall trend of resistances are similar across all the sections.

R_{ct} represents the sum of the anodic and cathodic charge transfer resistances ($R_{ct,a}$ and $R_{ct,c}$). Although the absolute values of resistances show variations between the three sections, the overall trend exhibits a steeper increase compared to ohmic resistance as testing progresses. The Impedance data show that R_{ct} remains statistically invariant during the first 320 h of operation followed by an increase. This suggests a delayed onset of interface restructuring, possibly linked to redeposition dynamics or electrolyte changes as the mechanisms involved. DRT analysis

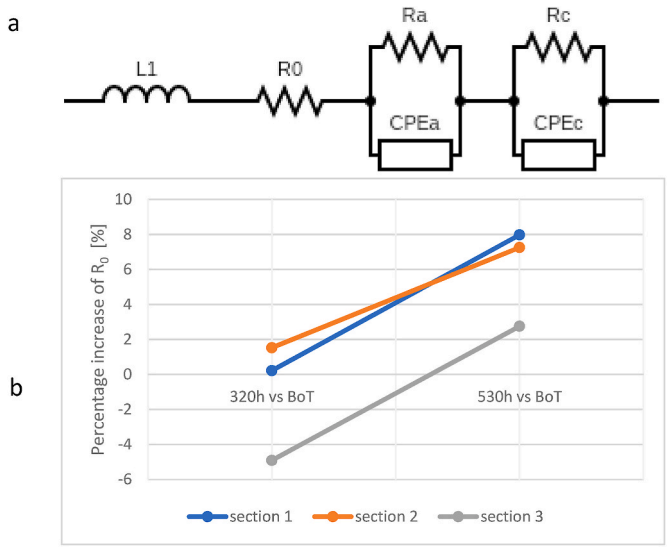

Fig. 7. a) Electrical equivalent circuit used to fit the test results. b) Percentage of increment of R_0 (high frequency resistance) in durability tests 320 h with respect to the BoT and at 530 h with respect to the BoT.

supports this trend and reveals increasing low-frequency polarization at later stages.

The change in total resistance results from a combined effect of both ohmic and charge transfer contributions. The total resistance does not change significantly in the test up to the 530 h, although a slight degradation can be observed up to this point of test. On the other hand, a small improvement can also be seen specially from BoT to 320 h. This timeframe (0–320 h) corresponds to the longest continuous durability test conducted. However, since EIS tests during these initial 320 h were performed only at the beginning and end of the period, it would be challenging to speculate the precise trend of different degradative phenomena and directly compare results from the durability test and EIS data. Nonetheless, what can be inevitably pointed out is the increasing trend of ohmic resistance that shows a continuous increment. This behaviour is also evident in the durability tests, suggesting that at least a portion of the degradation can be attributed to the rise in ohmic resistance. Besides, the increment in total resistance could suggest a trend of slowing down in the kinetics of reactions. Furthermore, electrochemical-impedance measurements corroborate the durability results. During the first 320 h of operation—which bracket the start and end of the longest uninterrupted 230 h block—the stack-averaged high-frequency resistance R_0 and total resistance R_{tot} changed by no more than 3 % and 21 %, respectively, across all three monitored sections. In the subsequent 190 h period (320–530 h) the same metrics remained equally stable, staying within 7 % (R_0) and 22 % (R_{tot}). The close agreement between these two time windows demonstrates homogeneous stack behaviour and shows that the scheduled shutdowns did not introduce measurable performance scatter. Consistently, the Nyquist spectra exhibited no new semicircle or low-frequency tail, ruling out mass-transport limitations throughout the test.

3.3.4. DRT

Distribution of Relaxation Time (DRT) analysis has been conducted on the EIS results presented in the previous section, following the methodology of T. H. Wan et al. [30]. Similar to the approach used for the equivalent circuit analysis, data reduction was applied by averaging the EIS data for each section of the stack. Specifically, for cells 3–13, the EIS data was averaged to produce a single Nyquist curve, which was then designated as the Distribution of Relaxation Time for section one. The same approach was applied to sections two and three, corresponding to cells 14–24 and 25–35, respectively. The analysis for these three sections has been done at 0h (BoT), 320h, and 530h (EoT).

Distribution of relaxation times for all the three sections of the stack at the beginning, middle (320h) and end of tests are brought in Fig. 8. The complete graphs as a function of time can also be seen in the supplementary materials. Although small variations may be seen in the graphs, based on the characteristic times (or frequencies) of electrochemical processes clear hypotheses can still be formulated regarding the assignment of peaks to the electrochemical phenomena occurring within the cells.

Taking into account the trend of the peaks, based on the literature and the stack condition, each peak has been assigned to a phenomenon according to the characteristic time of the corresponding peak region.

Peak three at ca. 10^{-2}- 10^{-3}[s] has been attributed to both anodic and cathodic ionic transport in the catalyst layer (Oxygen Evolution Reaction, OER and Hydrogen Evolution Reaction, HER). Peak two at ca. 10^{-1}-10^{-2}[s] corresponds to cathodic charge transfer of the Hydrogen Evolution Reaction (HER CT), while peak one at ca. 10° s has been attributed to anodic charge transfer of the Oxygen Evolution Reaction (OER CT). The peaks related to the first section of the stack are in some cases shifted towards lower frequencies. Nonetheless, they show the same pattern of the other sections. Two other singular behaviours have also been recognized with their probable relative phenomena. Peak x (first peak at 0h in the section one and at 530h in the section three of the stack) could be related to the transport processes (water, gas or mass). It could be due to problems related to transport phenomena considering that this section is the drier side of the stack where the liquid exit. On the other hand, at 530 h the tendency of peak separation between different ionic transport phenomena is seen which could be the separation of the faster cathodic HER ionic transport from the slower anodic OER ionic transport. The complete frequency range of detected peaks have been reported in Table 6.

The peaks' characteristic frequency has been compared to the work of Matthias Ranz et al. on the dynamics of anion exchange membrane electrolysis [31]. Considering this assigning hypothesis, the following behaviour is observed for each phenomenon:

- Ionic transport losses within catalyst layers exhibits an incremental increasing trend during the 530 h of the experiment.
- Cathodic charge transfer resistance increases from 0 to 320 h, after which the results remain approximately constant up to 530 h.
- Anodic charge transfer resistance shows a continuous decrease from 0 to 530 h.

This analysis is consistent with the findings of the electrical equivalent circuit analysis. It also highlights that, while the impact of ohmic resistance should never be underestimated, in the case of this AEM stack, the contribution of charge transfer resistance to the overall degradation of the cells is greater than expected. This has been confirmed by both DRT and EEC analyses.

3.4. Performance evaluation

The performance evaluation of the hybrid alkaline/membrane electrolysis cell designs was conducted to identify key performance metrics and operational characteristics. The study encompassed both single cells (not here reported) and stack configurations, focusing on efficiency, energy consumption, and hydrogen production rates under varying operating conditions.

3.4.1. The evaluation highlighted several important KPIs

- Stack efficiency: measured at various pressures and temperatures, the stack efficiency ranged between 72 % and 81 % at 1 bar, with higher pressures resulting in lower efficiencies due to increased energy demands.

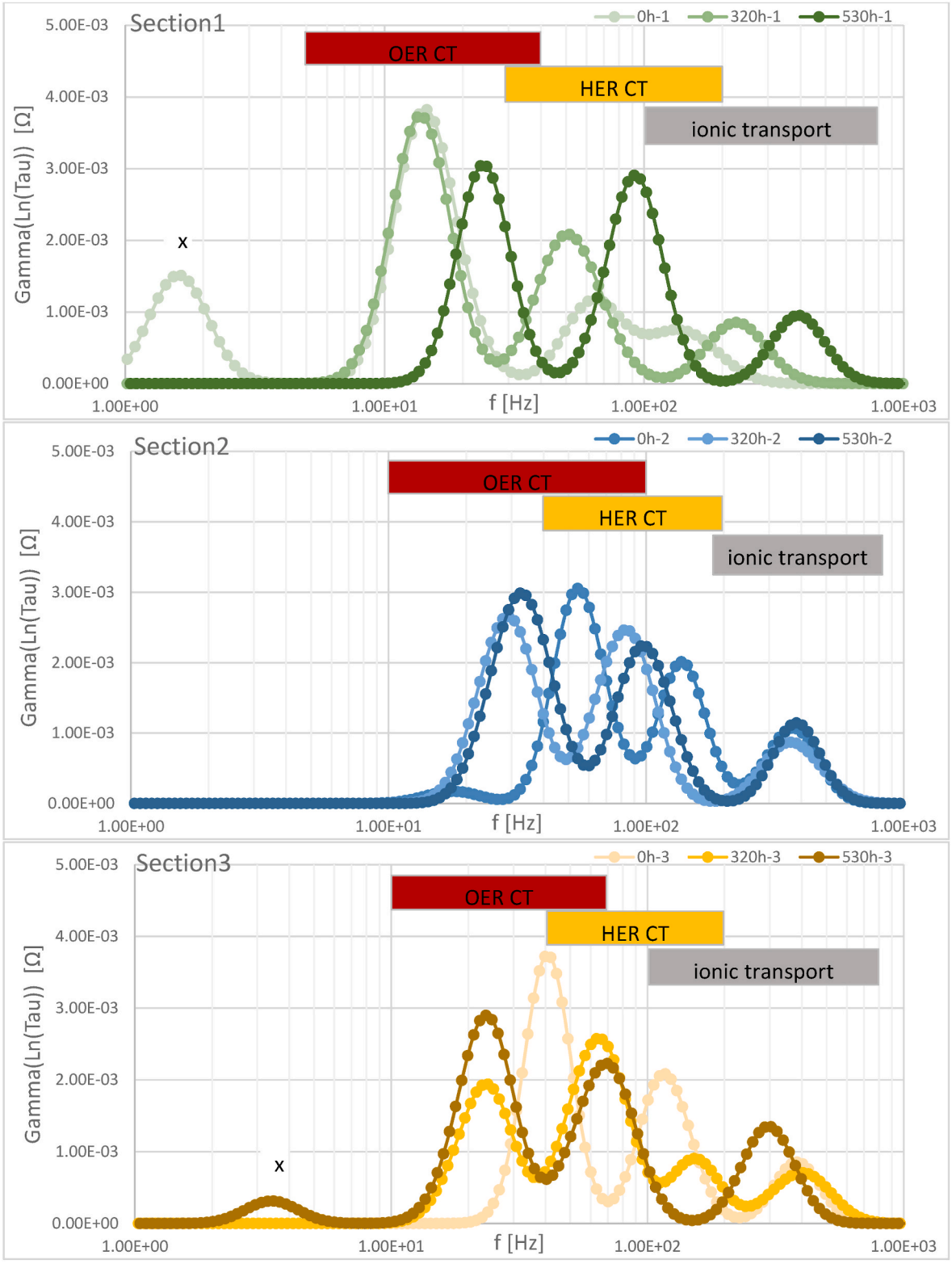

Fig. 8. DRT for the three sections of the stack from BoT to EoT.

- Specific energy consumption: the specific energy consumption varied between 41 and 50 kWh/kg, depending on the operating pressure and current density. Tests at 1 bar demonstrated the most energy-efficient operation, with values nearing the 2050 target for green hydrogen production.
- Hydrogen purity: oxygen contamination in the hydrogen stream decreased significantly at higher pressures, with levels ranging from 30 ppm at 1 bar to below 10 ppm at 10 bar, indicating enhanced gas separation efficiency in pressurized operations.
- Degradation trends: over the course of approximately 500 h of operation, the system exhibited both reversible and irreversible degradation phenomena. Analysis showed that reversible degradation was recoverable during rest periods, while irreversible

Table 6
frequency range of peaks.

Peak No	Process	Frequency range [Hz]	
1	OER charge transfer	5	100
2	HER charge transfer	30	200
3	Ionic transport losses within catalyst layers	100	800

degradation was primarily attributed to membrane and catalyst layer deterioration.

3.4.2. EIS analysis

EIS measurements conducted during durability tests provided insights into the resistance components and degradation mechanisms. Key findings included:

- an increase in ohmic resistance over time, corresponding to membrane and electrode wear.
- a rise in charge transfer resistance, particularly on the anode side, indicating potential degradation of the oxygen evolution reaction catalyst.

3.5. Implications for scale-up

Scaling up the hybrid electrolysis technology from lab-scale to industrial-scale applications involves addressing challenges in system design, operational stability, and economic viability. The following considerations highlight critical factors for successful scale-up:

3.5.1. Technical considerations

- Stack design optimization: the use of mechanically supported membranes ensures robustness under high-pressure conditions, reducing the risk of hydrogen crossover. However, achieving uniform current distribution and effective water management in larger stacks will be crucial.
- Material selection: the adoption of cost-effective, durable catalysts and membranes is critical. The development of non-precious metal catalysts and reinforced membranes for long-term durability will help meet industrial demands.
- Modular Design: a modular approach to stack construction will facilitate scalability while maintaining performance consistency. Modular systems also simplify maintenance and reduce downtime.

3.5.2. Economic considerations

- Cost efficiency: the hybrid design significantly reduces costs by enabling the use of non-precious or low PGM catalysts and simplified balance-of-plant (BoP) components. Scale-up efforts must prioritize minimizing capital and operational costs to ensure economic competitiveness.
- Energy efficiency: achieving specific energy consumption levels below 45 kWh/kg is essential for aligning with future industrial benchmarks. Optimized operating conditions and advanced control systems will be necessary to achieve these targets.
- Market integration: the hybrid technology's compatibility with intermittent renewable energy sources (e.g., solar and wind) positions it as an ideal solution for green hydrogen production.

3.5.3. Operational considerations

- Durability and maintenance: long-term durability tests indicate the need for operation and maintenance strategies to manage reversible degradation and prevent irreversible damage. Adaptive operational strategies, such as intermittent operation and regular system checks, can enhance system longevity.
- Safety protocols: high-pressure operation necessitates stringent safety measures, including robust monitoring and control systems, to mitigate risks associated with hydrogen leakage or system failure.

4. Conclusions

This work evaluated the KPIs and durability at the stack level in a hybrid AEMWE configuration, utilizing a robust design of experiments approach. The main conclusions can be summarized as follows:

- The 1st generation stack showed a stack specific consumption already below the SoA (2020) values reported by IRENA and a system specific consumption in nominal conditions better than the SoA (2020) of the SRIA and close to the 2024 adjusted SRIA target, with a higher current density level than the SRIA target (1 A/cm^2 vs 0.6 A/cm^2) even with a non-optimized BoP.
- The 2nd generation stack tested at 10 bar showed a performance also better than the SoA (2020) reported by IRENA, but worse than the 1st generation stack and the SRIA SoA (2020) adjusted value at system level.
- When tested at 1 bar, the 2nd generation demonstrated a specific consumption at system level already better than the SRIA target for 2024, at three different temperatures and for a current density higher than the 2024 SRIA target (1 A/cm^2 vs 0.6 A/cm^2), even with a not optimized BoP. The 2nd generation shows also a stack specific consumption already lower than the SoA (2020) level reported by IRENA for the AEMWE technology. In the case of the 1 bar test at the higher temperature (around 67 °C stack outlet), the stack achieved a specific consumption already close to the 2050 target reported by IRENA, even if the target refers to a higher current density (>2 A/cm^2) and a higher pressure (>70 bar).
- The stack proved to be reliable and capable of operating continuously for hundreds of hours. Unfortunately, multiple interruptions occurred during the long-term operation but none of these was caused by a failure in the stack. When comparing the results of the durability test with the existing literature clearly emerges that the experimental campaign was conducted adopting very rigorous testing conditions (i.e., current density and operating pressure).
- The analysis of the different test intervals highlighted that a significant share of the degradation is recovered after interrupting and restarting the system. When considering only the permanent degradation, the percentage voltage increase after 1000 h results in 1.35 %, which is close to the SRIA target for 2024 (i.e., 0.9 %/1000 h).
- EIS tests were conducted on each cell of the stack at the start, middle and end of the durability test. Equivalent circuit model and distribution of relaxation times were studied. Analysis of EIS indicated a progressive increase in ohmic resistance over time that could be associated with membrane and electrode degradation, although a slight improvement has been observed initially. Moreover, EIS revealed an increase in charge transfer resistance, especially on the anode side, suggesting potential deterioration of the oxygen evolution reaction catalyst. This observation has been confirmed by DRT. To the best of the authors' knowledge, analysis on the EEC and DRT of AEM stacks is absent in the literature.

CRediT authorship contribution statement

Domenico Ferrero: Writing – original draft, Visualization, Software, Methodology, Formal analysis, Data curation, Conceptualization. **Mohsen Mansourkiaei:** Writing – original draft, Visualization, Software, Methodology, Formal analysis, Data curation, Conceptualization. **Davide Trapani:** Writing – original draft, Visualization, Software, Methodology, Formal analysis, Data curation, Conceptualization. **Daniele Consoli:** Writing – review & editing, Methodology, Conceptualization. **Paolo Prevedello:** Writing – review & editing, Methodology, Conceptualization. **Ignazio Assenza:** Writing – review & editing,

Methodology, Conceptualization. **Paul Matter:** Writing – review & editing, Writing – original draft, Resources, Methodology, Investigation, Data curation, Conceptualization. **Travis Hery:** Writing – review & editing, Resources, Investigation. **Mahtab Fox:** Writing – review & editing, Resources, Investigation. **Alessandro Monteverde:** Writing – review & editing, Writing – original draft, Software, Methodology, Formal analysis, Conceptualization. **Massimo Santarelli:** Writing – review & editing, Writing – original draft, Supervision, Project administration, Methodology, Funding acquisition, Formal analysis, Conceptualization.

Declaration of competing interest

The authors declare that they have no known competing financial interests or personal relationships that could have appeared to influence the work reported in this paper.

Acknowledgements

The authors gratefully acknowledge the support provided by the Nexthy Booster Program from Enel Green Power S.p.A.

Acronyms

AWE	Alkaline electrolyzer
AEMWE	Anion exchange membrane electrolyzer
BoI	Beginning of interval
BoP	Balance of plant
BoT	Beginning of test
CPE	Constant phase elements
DoE	Design of experiment
DRT	Distribution of relaxation time
EEC	Electrical equivalent circuit
EIS	Electrochemical impedance spectroscopy
EoI	End of interval
EoT	End of test
GDE	Gas diffusion electrodes
GDL	Gas diffusion layer
HER	Hydrogen evolution reaction
IRENA	International Renewable Energy Agency
KK	Kramers-Kronig
KPI	Key performance indicators
LHV	Lower heating value
NNM	Non-noble metal
OER	Oxygen evolution reaction
P2H2	Power to hydrogen
PEMWE	Proton exchange membrane electrolyzer
PGM	Platinum-group metals
SLPM	Standard liter per minute
SoA	State of the art
SRIA	Strategic Research and Innovation Agenda

Appendix A. Test protocols

The test protocol of stack performance tests is reported in Table A.1.

Table A.1
Description of test protocol of stack performance test

Step #	Step description
1	Start the system (standard starting procedure defined by Producer) and impose the nominal stack power as final setpoint
2	Wait for end of start-up protocol to reach nominal power
3	Wait for system power to stabilize by ± 5 % in a 15 min interval
4	Set the power level to the set-point value P_{sp}
5	Wait the stack power to stabilize. The system is considered stable if the average power of two consecutive intervals of 60 s does not differ by more than ±2 % $P_{stack,\ average}$
6	Keep the state for at least 15 min with power variation below ±5 % $P_{stack,\ average}$
7	Repeat steps 4–6 for other Power set-points if the system must be tested in more than one Power level
8	End of test

Appendix B. Stack performance results

The results of stack performance tests are reported in Table B.1, Table B.2 and Table B.3.

Table B.1
Stack test KPIs – first generation stack (10 bar, Thigh)

	P1	*P2*	*P3*	
Power	2500	5000	6319	***W***
Current	42.67	81.51	101.00	***A***
Voltage	58.58	61.34	62.57	***V***
Average Cell Voltage	1.63	1.70	1.74	***V/cell***
Hydrogen production rate	10.20	19.89	24.64	***SLPM***
Hydrogen production rate	0.05	0.11	0.13	***kg/h***
Stack Efficiency	72.8 %	70.9 %	69.5 %	
Stack Specific Energy Consumption	45.76	46.95	47.91	***kWh/kg***
System Efficiency	59.5 %	61.4 %	60.9 %	
System Specific Energy consumption	55.94	54.22	54.65	***kWh/kg***
H_2 purity (O_2 content)	31.83	32.56	32.60	***ppm***
H_2 purity (H_2O content)	684.12	604.02	457.54	***ppm***
O_2 purity (H_2 content)	2.85	2.94	3.55	***ppm***
Average Outlet Temperature	66.4	68.1	69.2	***°C***

Table B.2
Stack tests KPIs – second generation stack (1 bar)

KPI	Test @ 57 °C			Test @ 62 °C			Test @ 67 °C			Unit
	P1	P2	P3	P1	P2	P3	P1	P2*	P3*	
Power	2500	5000	6381	2500	5000	6500	2500	5000	6458	***W***
Current	42.30	80.06	100.00	41.79	78.40	98.71	42.31	79.70	100.00	***A***
Voltage	59.11	62.46	63.81	59.82	63.78	65.85	59.08	62.73	64.59	***V***
Average Cell Voltage	1.64	1.73	1.77	1.66	1.77	1.83	1.64	1.74	1.79	***V/cell***
Hydrogen production rate	10.75	20.28	26.06	10.49	21.40	26.96	11.35	21.45	27.49	***SLPM***
Hydrogen production rate	0.06	0.11	0.14	0.06	0.11	0.14	0.06	0.11	0.15	***kg/h***
Stack Efficiency	77 %	72 %	73 %	80 %	76 %	74 %	81 %	76 %	76 %	
Stack Specific Energy Consumption	43.44	46.06	45.79	41.89	43.65	45.04	41.21	43.60	43.91	***kWh/kg***
System Efficiency	63 %	63 %	64 %	65 %	66 %	65 %	66 %	66 %	67 %	
System Specific Energy Consumption	53.1	53.2	52.2	51.2	50.4	51.3	50.4	50.3	50.0	***kWh/kg***
H_2 purity (O_2 content)	155.92	78.04	74.63	112.80	100.27	96.58	168.05	66.24	38.54	***ppm***
H_2 purity (H_2O content)	18568	16389	18006	19355	20950	20519	21262	20215	20522	***ppm***
O_2 purity (H_2 content)	5.30	8.19	12.24	4.32	4.76	5.51	1.86	1.66	2.73	***ppm***
Average Outlet Temperature	59.4	61.0	60.9	59.3	61.2	61.3	65.4	66.8	66.7	***°C***

*P2 and P3 test are the average of 2 repetitions, because the 3rd repetition was excluded due to an anomalous hydrogen flow recording.

Table B.3
Stack tests KPIs – second generation stack (10 bar)

KPI	Test @ 62 °C	Test @ 67 °C			Unit
	P3	P1	P2	P3	
Power	6223	2500	5000	6487	***W***
Current	99.41	41.83	79.00	99.41	***A***
Voltage	65.26	59.76	63.29	65.26	***V***
Average Cell Voltage	1.81	1.66	1.76	1.81	***V/cell***
Hydrogen production rate	23.74	10.07	19.40	24.57	***SLPM***
Hydrogen production rate	0.13	0.05	0.10	0.13	***kg/h***
Stack Efficiency	68 %	72 %	69 %	68 %	
Stack Specific Energy Consumption	48.96	46.38	48.13	49.32	***kWh/kg***
System Efficiency	58 %	59 %	60 %	59 %	
System Specific Energy Consumption	57.4	56.7	55.6	56.2	***kWh/kg***
H_2 purity (O_2 content)	8.18	27.88	8.69	8.18	***ppm***
H_2 purity (H_2O content)	12319	12485	11648	12319	***ppm***
O_2 purity (H_2 content)	8.01	4.78	3.65	8.01	***ppm***
Average Outlet Temperature	62.7	66.5	67.0	66.7	***°C***

Appendix A. Supplementary data

Supplementary data to this article can be found online at https://doi.org/10.1016/j.jpowsour.2025.238239.

Data availability

The data that has been used is confidential.

References

[1] E.K. Volk, M.E. Kreider, S. Kwon, S.M. Alia, Recent Progress in Understanding the Catalyst Layer in Anion Exchange Membrane Electrolyzers – Durability, Utilization, and Integration, Royal Society of Chemistry, Jan. 01, 2024, https://doi.org/10.1039/d3ey00193h.

[2] M. Ranz, B. Grabner, B. Schweighofer, H. Wegleiter, A. Trattner, Dynamics of anion exchange membrane electrolysis: unravelling loss mechanisms with electrochemical impedance spectroscopy, reference electrodes and distribution of relaxation times, J. Power Sources 605 (Jun. 2024), https://doi.org/10.1016/j.jpowsour.2024.234455.

[3] Y.S. Park, et al., Commercial anion exchange membrane water electrolyzer stack through non-precious metal electrocatalysts, Appl. Catal., B 292 (Sep. 2021), https://doi.org/10.1016/j.apcatb.2021.120170.

[4] A.W. Tricker, J.K. Lee, J.R. Shin, N. Danilovic, A.Z. Weber, X. Peng, Design and operating principles for high-performing anion exchange membrane water electrolyzers, J. Power Sources 567 (May 2023), https://doi.org/10.1016/j.jpowsour.2023.232967.

[5] R. Vinodh, T. Palanivel, S.S. Kalanur, B.G. Pollet, Recent Advancements in Catalyst Coated Membranes for Water Electrolysis: a Critical Review, Royal Society of Chemistry, May 08, 2024, https://doi.org/10.1039/d4ya00143e.

[6] G.H.A. Wijaya, K.S. Im, S.Y. Nam, Advancements in Commercial Anion Exchange Membranes: a Review of Membrane Properties in Water Electrolysis Applications, Elsevier B.V., Oct. 01, 2024, https://doi.org/10.1016/j.dwt.2024.100605.

[7] S. Koch, et al., Water management in anion-exchange membrane water electrolyzers under dry cathode operation, RSC Adv. 12 (32) (Jul. 2022) 20778–20784, https://doi.org/10.1039/d2ra03846c.

[8] N.U. Hassan, et al., Effect of porous transport layer properties on the anode electrode in anion exchange membrane electrolyzers, J. Power Sources 555 (Jan. 2023), https://doi.org/10.1016/j.jpowsour.2022.232371.

[9] H. Ito, N. Kawaguchi, S. Someya, T. Munakata, Pressurized operation of anion exchange membrane water electrolysis, Electrochim. Acta 297 (Feb. 2019) 188–196, https://doi.org/10.1016/j.electacta.2018.11.077.

[10] M. Beachy, C. Holt, M. Ocampo, P. Matter, Electrochemical Cell and Method of Using Same, Apr. 19, 2018, 10,844,497 B2.

[11] M. Beachy, C. Holt, M. Ocampo, P. Matter, Electrochemical Cell and Method of Using Same, Oct. 19, 2020, 11,228,051 B2.

[12] S. Bin Park, J.E. Park, G. Na, C. Choi, Y.H. Cho, Y.E. Sung, Low-cost and high-performance anion-exchange membrane water electrolysis stack using non-noble metal-based materials, ACS Appl. Energy Mater. 6 (17) (Sep. 2023) 8738–8748, https://doi.org/10.1021/acsaem.3c01215.

[13] M.J. Jang, et al., Efficient and durable anion exchange membrane water electrolysis for a commercially available electrolyzer stack using alkaline electrolyte, ACS Energy Lett. 7 (8) (Aug. 2022) 2576–2583, https://doi.org/10.1021/acsenergylett.2c01049.

[14] M. Moreno-González, et al., One year operation of an anion exchange membrane water electrolyzer utilizing Aemion+® membrane: minimal degradation, low H2 crossover and high efficiency, J. Power Sour. Advan. 19 (Jan. 2023), https://doi.org/10.1016/j.powera.2023.100109.

[15] C. Hu, et al., Reinforced poly(dibenzyl-co-terphenyl piperidinium) membranes for highly durable anion-exchange membrane water electrolysis at 2 A cm−2 for 1000 h, Next Energy 1 (3) (Sep. 2023) 100044, https://doi.org/10.1016/j.nxener.2023.100044.

[16] J. Wang, et al., Durable and conductive anion exchange membranes based on Poly (m-triphenyl carbazolyl piperidinium) for water electrolysis, Int. J. Hydrogen Energy 58 (Mar. 2024) 514–524, https://doi.org/10.1016/j.ijhydene.2024.01.161.

[17] X. Hao, X. Wu, Q. Pan, T. Xiu, Z. Zhang, H. Qian, Simulation of a pressurized alkaline water electrolysis electrolyzer cell and its system, ACS Omega 10 (22) (Jun. 2025) 23750–23763, https://doi.org/10.1021/acsomega.5c02476.

[18] G. Tsotridis, A. Pilenga, EU Harmonised Protocols for Testing of Low Temperature Water Electrolysers, 2021, https://doi.org/10.2760/58880.

[19] ANIONE project, D2.1 Harmonised test protocols for assessing AEM electrolysis components, cells and stacks in a wide range of operating temperature and pressure [Online]. Available: www.anione.eu, 2020.

[20] J. Xing, et al., Long-term durability test of highly efficient membrane electrode assemblies for anion exchange membrane seawater electrolyzers, J. Power Sources 558 (Feb. 2023), https://doi.org/10.1016/j.jpowsour.2022.232564.

[21] P. Gazdzick, J. Mitzel, D. Garcia Sanchez, M. Schulze, K.A. Friedrich, Evaluation of reversible and irreversible degradation rates of polymer electrolyte membrane fuel cells tested in automotive conditions, J. Power Sources 327 (Sep. 2016) 86–95, https://doi.org/10.1016/j.jpowsour.2016.07.049.

[22] Green hydrogen cost reduction scaling up electrolysers to meet the 1.5°C climate goal H 2 O 2 [Online]. Available: www.irena.org/publications, 2020.

[23] Clean Hydrogen JU SRIA - Approved by GB - Clean for Publication (ID 13246486)"..

[24] Clean Hydrogen Joint Undertaking, Strategic Research and Innovation Agenda 2021 – 2027, 2022.

[25] D. Li, et al., Durability of anion exchange membrane water electrolyzers, Energy Environ. Sci. 14 (6) (Jun. 2021) 3393–3419, https://doi.org/10.1039/d0ee04086j.

[26] L.J. Titheridge, A.T. Marshall, The rationale for a standardized testing protocol for anion exchange membrane water electrolyzers, Am. Chem. Soc. (Mar. 08, 2024), https://doi.org/10.1021/acsenergylett.4c00239.

[27] N. Du, C. Roy, R. Peach, M. Turnbull, S. Thiele, C. Bock, Anion-exchange membrane water electrolyzers, Am. Chem. Soc. (Jul. 13, 2022), https://doi.org/10.1021/acs.chemrev.1c00854.

[28] M. Schönleber, D. Klotz, E. Ivers-Tiffée, A method for improving the robustness of linear kramers-kronig validity tests, Electrochim. Acta 131 (2014) 20–27, https://doi.org/10.1016/j.electacta.2014.01.034.

[29] B.A. Boukamp, A linear kronig-kramers transform test for immittance data validation, J. Electrochem. Soc. 142 (6) (1995) 1885–1894, https://doi.org/10.1149/1.2044210.

[30] T.H. Wan, M. Saccoccio, C. Chen, F. Ciucci, Influence of the discretization methods on the distribution of relaxation times deconvolution: implementing radial basis functions with DRTtools, Electrochim. Acta 184 (Dec. 2015) 483–499, https://doi.org/10.1016/j.electacta.2015.09.097.

[31] M. Ranz, B. Grabner, B. Schweighofer, H. Wegleiter, A. Trattner, Dynamics of anion exchange membrane electrolysis: unravelling loss mechanisms with electrochemical impedance spectroscopy, reference electrodes and distribution of relaxation times, J. Power Sources 605 (Jun. 2024), https://doi.org/10.1016/j.jpowsour.2024.234455.